Supramolecular Chemistry

DOI: 10.1002/anie.201109162

Concave versus Planar Geometries for the Hierarchical Organization of Mesoscopic 3D Helical Fibers**

Juan Luis López, Carmen Atienza, Alberto Insuasty, Javier López-Andarias, Carlos Romero-Nieto, Dirk M. Guldi, and Nazario Martín**

Dedicated to Professor Miguel A. Alario on the occasion of his 70th birthday

Constructing suitably functionalized supramolecular ensembles at different length scales from molecular building blocks that feature electronic and/or optic activity constitutes a major challenge in contemporary science.[1] To this end, the hierarchical control over self-organizing constituents that evolve into 1D nanostructures, 2D, and 3D nanocrystallites—all of them with new electronic properties—is at the forefront.[2] Leading examples of truly sophisticated 1D, 2D, and 3D architectures comprising photo- and redoxactive constituents feature planarity as a common templating motif.[3] Notable exceptions are spherical fullerenes and concave curved polycyclic aromatic hydrocarbons (PAHs).[4,5]

Importantly, helical nanostructures of mesoscopic dimensions are abundant in biology and are usually composed by helical fibrils that often assemble into highly ordered hierarchical materials. This triggered tremendous interest during the last decade to create artificial helical nanostructures that range from 1 to 100 nm.[6] One of the most interesting types of building blocks is bioinspired peptide amphiphiles (PAs). Critical to the design is to place bulky and non-stackable substituents, which introduce considerable torsional strain, in close proximity to the β-sheet-forming peptide sequences. As a matter of fact, the systems tend to collapse into superhelixes under solvophobic conditions.[6c,d] Specifically a significant number of aromatic peptide amphiphilic systems have been used to organize planar chromophores into chiral arrays during the last years.[7] Most of these cases rely, however, on constructing helical assemblies of only a few nanometers.[8] Few examples dealing with the hierarchical growth of highly ordered helical materials at mesoscopic scales have been reported so far.[9]

Recently, we have shown that curved 9,10-di(1,3-dithiol-2-ylidene)-9,10-dihydroanthracene (exTTF) facilitates the formation of 3D multilamellar supramolecular helical assemblies.[10] We have shown that π–π interactions between non-planar exTTFs augmented by van der Waals interactions between long side chains are able to stabilize tertiary structures (i.e., twisted flat ribbonlike structures) that further assemble into higher-order 3D helical nanofibers as a consequence of a solvophobic collapse. In the ground state, the properties of the exTTF stemming from this type of 3D nanostructure environment featured absorption bands that are bathocromically shifted with respect to the absorption bands of pristine exTTF. In the excited state, a new delocalized electronic state results from efficient intermolecular π–π interactions between exTTF units.

In this context, the present work focuses on determining the effects of non-planar exTTFs—with their concave-shaped central moiety—on the growth of new supramolecular 3D architectures at different length scales. Furthermore, a comparison with related but more-planar structures enables dissecting the influences of the shape on the chirality of the resulting mesostructures. In particular, we have designed and synthesized three precursors based on aromatic peptide amphiphilic systems (**1a–c**) with alanyl-glycyl-alanyl-glycyl-alanine (AGAGA) pentapeptide sequences that are linked to fluorene, anthracene, and exTTF (Figure 1A).

On one hand, the presence of short peptide sequences eases the formation of chiral β sheets as secondary structure.[7,8,11] In fact, we hypothesize that the introduction of bulky exTTFs in **1c**, with its concave central core near the β-sheet-forming peptide sequences, induces torsional strains in the secondary H-bonded nanostructure. The consequences are twofold: firstly, a maximum intermolecular H bonding within the peptide backbone is preserved. Secondly, mutual interactions between exTTFs are avoided. In turn, 1D helical nanostructures are realized at the nanoscale driven exclusively by H-bonding interactions. The latter seem to be susceptible to a subsequent self-assembly process at mesoscopic length scales. In fact, π–π interacting exTTFs merge under solvophobic conditions into 3D highly ordered hierarchical architectures with helical features (see Figure 1C).

[*] Dr. J. L. López, Dr. C. Atienza, A. Insuasty, J. López-Andarias, Prof. N. Martín
Departamento de Química Orgánica, Facultad de C. C. Químicas
Universidad Complutense de Madrid, 28040 Madrid (Spain)
and
IMDEA-nanociencia, 28049 Madrid (Spain)
E-mail: nazmar@quim.ucm.es
Homepage: http://www.ucm.es/info/fullerene
Dr. C. Romero-Nieto, Prof. D. M. Guldi
Department of Chemistry and Pharmacy & Interdisciplinary Center for Molecular Materials
University of Erlangen-Nuremberg
Egerlandstraße 3, 91058 Erlangen (Germany)

[**] Financial support by the Ministerio de Ciencia e Innovación (MICINN) of Spain (project numbers CTQ2011-24652 and Consolider-Ingenio CSD2007-00010), the EU (FUNMOLS FP7-212942-1) the CAM (MADRISOLAR-2 project S2009/PPQ-1533) is acknowledged. We also thank to the Deutsche Forschungsgemeinschaft (SFB583). The MICINN of Spain is thanked by C.A. for a Ramón y Cajal contract.

Supporting information for this article is available on the WWW under http://dx.doi.org/10.1002/anie.201109162.

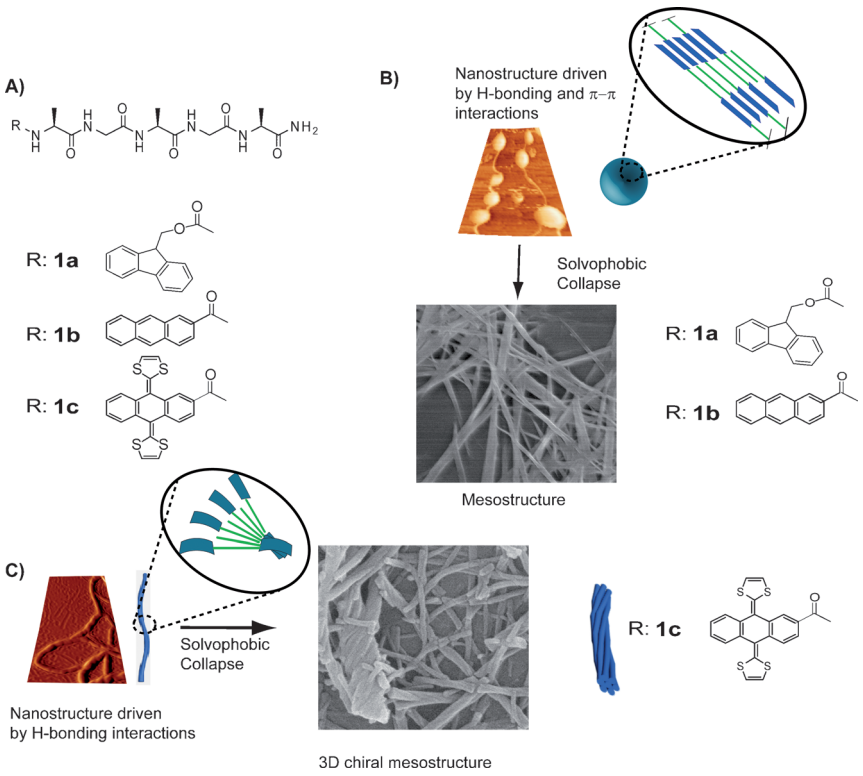

Figure 1. A) Structures of **1a–c**. B and C) Proposed models for the growth of architectures at different length scales (i.e., primary, secondary, and tertiary) for **1a–c**.

Implicit is that the chirality of the peptide is efficiently expressed in the 3D mesoarchitecture.

On the contrary, less-bulky planar aromatic cores, such as fluorene **1a** and/or anthracene **1b**, near the β-sheet-forming peptide sequences, reduce the torsional strains in the primary assembly. As a matter of fact, under the same solvophobic conditions, control over the growth of mesoarchitectures is complicated and helicity is lacking. Please note that in these planar systems the chirality of the peptide is not expressed in the nanostructure—similarly to recently reported systems (Figure 1B).[7]

Therefore, we expect that the different geometric aromatic cores in **1a–c**, that is, planar aromatic cores (**1a** and **1b**) versus concave aromatic cores (**1c**), would give rise to remarkable differences in the growth and morphologies of the primary, secondary, and tertiary structures.

The syntheses of **1b** and **1c** were carried out by linking the corresponding carboxylic acid derivatives to N-terminated amine pentapeptides—see the Supporting Information. **1a** was synthesized by standard fluorenylmethoxycarbonyl (Fmoc) mediated solid-phase synthesis on a 4-methylbenzhydrylamine (MBHA) resin. Removal of the Fmoc group and subsequent cleavage from the resin afforded the AGAGA peptide, bearing amine and amide groups at the N- and C-termini, respectively. The product was precipitated in cooled ether and was used without further purification for the final coupling steps. The structural characterizations of **1a–c** were achieved by standard spectroscopic techniques—for more details see the Supporting Information.

FTIR measurements of **1a–c** in halogenated solvents such as chloroform ($CHCl_3$) and tetrachloroethane ($C_2H_2Cl_4$) featured intense peaks for amide I at around 1629 cm^{-1} and weaker shoulders at around 1690 cm^{-1} as a corroboration for intermolecular β sheets in the peptide backbone, in which the peptide units are interacting antiparallel (see Figure S1 in the Supporting Information). Fluorescence experiments in $C_2H_2Cl_4$ with **1a** and **1b** showed quenching because of planar aromatics that are π–π interacting (Figure S2 in the Supporting Information).[7b]

On the contrary, the absorption spectrum of **1c**—bearing a concave nonplanar exTTF unit—gives rise to only a small bathochromic shift of 5 nm in, for example, $CHCl_3$. Such a shift is far from what has previously been observed as an attest for π–π interacting exTTFs in supramolecular ensembles (see Figure S3 in the Supporting Information).[10]

These preliminary insights were further corroborated by microscopic assays. In this regard, AFM measurements from diluted $CHCl_3$ solutions of **1a** and **1b** drop-casted onto mica surfaces showed in both cases, the presence of homogeneous nanospheres with diameters over 30 nm (Figure S4A and S4B in the Supporting Information) and flat sheets with thicknesses of about 8 nm (Figure S5 in the Supporting Information). However, no discernible helical twists were noticed. In addition, XRD data of dried films of **1a** and **1b** suggest that the nanostructures formed are composed of several interlocked β-sheet arrangements (Figure 1B and Figure S6 in the Supporting Information). In line with previous reports we relate the growth of such nanostructures to H-bonding and π–π interactions.[7,8]

On the other hand, predominately curved, ropelike fibrils with diameters that range from 2 to 10 nm and with twisted shapes are seen for **1c** under the same experimental conditions (Figure 2A and 2B). It is remarkable that no tape, ribbonlike supramolecular ensembles were seen (Figure S7 in the Supporting Information). Circular dichroism (CD) experiments in $CHCl_3$ and $C_2H_2Cl_4$ displayed notable negative Cotton effects in the range of exTTF absorptions (Figure 2C). Such an observation is in good agreement with the existence of supramolecular aggregates, in which a transfer of chirality occurs from the peptides to the exTTFs.

It is interesting to note that in ropelike fibrils no exTTF interactions emerge, which is in agreement with the absorption spectra in halogenated solvents. As a matter of fact, intermolecular H-bonding interactions between peptide backbones remain as the driving force for the nanostructuring that was observed under these experimental conditions (Figure 2D). Unfortunately, the strong absorption of exTTF hampered any meaningful CD analysis of the peptide backbone. XRD studies, on the other hand, indicated the lack of

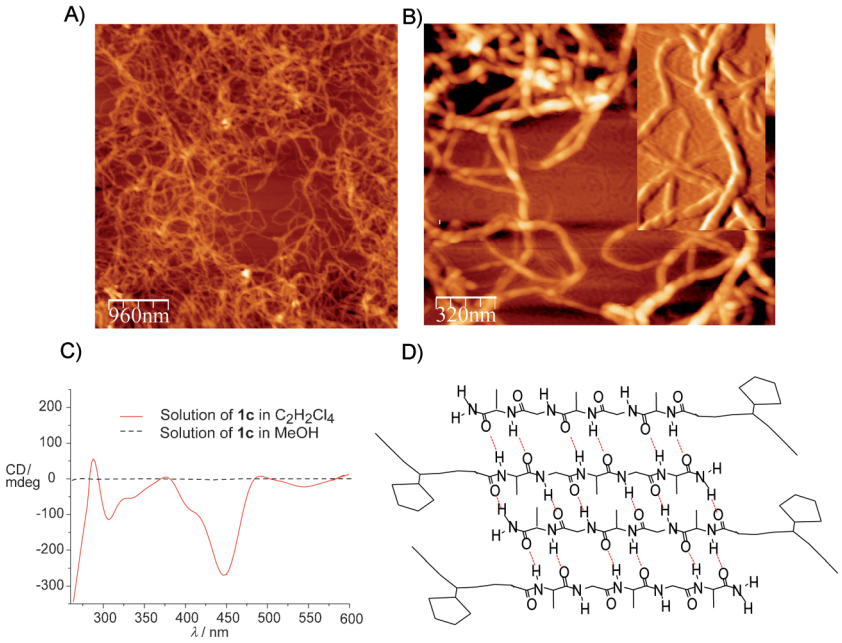

Figure 2. A and B) AFM images of **1c** from $C_2H_2Cl_4$ solutions on mica surfaces (5 μm × 5 μm and 1.6 μm × 1.6 μm). C) CD spectra of **1c** in MeOH (black spectrum) and in $C_2H_2Cl_4$ (red spectrum). D) Proposed secondary structure (i.e. β-sheet arrangements in antiparallel fashion) of **1c** in halogenated solvents.

long-range order in the supramolecular fibers that were formed in $CHCl_3$ and $C_2H_2Cl_4$ (Figure S8 in the Supporting Information).

In summary, the supramolecular, non-helical growth of **1a** and **1b**—bearing less-bulky planar aromatic rings—at the nanoscale length in halogenated solvents is mainly governed by H-bonding and π–π interactions, which is in agreement with previous reports.[8,10] On the contrary, for **1c**—bearing bulky non-planar exTTFs—the nanostructure growth is a consequence of intermolecular H-bonding interactions between peptide units. The latter leads to helical features in the secondary nanostructure.

In light of the aforementioned, we tested the peculiar non-planar shape of exTTF as a means to create tertiary structures, that is, mesoscopic 3D helical nanoarchitectures. We rationalized that the solvophobic collapse of the nanometric ropelike fibrils formed in halogenated solvents would promote intermolecular π–π interactions between exTTFs. The latter would be the inception to assemble these fibrils into mesoscopic helical materials, in which the helical handedness is controlled by the peptides. Such a type of growth control at different length scales is, to the best of our knowledge, unprecedented for this type of systems.

To this end, we aged **1c** in a solvent mixture of $CHCl_3$ and methylcyclohexane (MCH).[12] After one week, the absorption spectra showed large bathocromic shifts of the lower energy band from 450 to 500 nm and a concomitant decrease of the initial absorption band (Figure S9 in the Supporting Information). Such a bathocromic shift of around 50 nm is similar to our previously reported system and attests to π–π interacting exTTFs in the newly supramolecular ensemble.[10] It is remarkable that adding a few drops of MeOH to aged **1c** resulted in a quantitative recovery of the initial exTTF absorptions. These observations point to the overall reversibility of the process (Figure S10 in the Supporting Information).

As a complement to the aforementioned steady-state absorption measurements, which unambiguously confirm the transformation of **1c** (MeOH) into aged **1c** (MCH), we employed transient absorption measurements with **1c** in MeOH and aged **1c** in MCH (Figures S11 and S12 in the Supporting Information). In particular, 387 nm photoexcitation of **1c** in MeOH leads to the instantaneous formation of a transient that features a strong minimum at 440 nm, a strong maxima at 500 nm, and a series of weaker maxima at 730, 805, 930, 1000, 1035, and 1150 nm. Notable is that the 440 nm minimum is a good match of the exTTF-centered absorption seen in the ground state. With a rate of $6.6 \times 10^{11}\ s^{-1}$ all of the above features have decayed into a new and weak transition that maximizes around 550 nm. The latter decays with rate constant of $8.1 \times 10^{9}\ s^{-1}$ during which the ground state is completely reinstated. Implicit are ultrafast deactivations of excited states that are centered exclusively at exTTF. The presence of sulfur atoms is responsible for a second-order spin order coupling.

The transient absorption changes with aged **1c** in MCH upon excitation at 387 nm are quite different. Firstly, two minima—instead of just one—are discernable, namely at 455 and 560 nm, which again reflect the ground-state absorption of **1c**. Secondly, in the visible only a 495 nm maximum is seen, whereas the near-infrared is best characterized by a rather broad feature that spans from around 600 nm all the way to 1200 nm. Thirdly, the kinetics in the visible range give rise to a fast (i.e., $1.8 \times 10^{11}\ s^{-1}$) and a slow (i.e., $1.2 \times 10^{9}\ s^{-1}$) process to yield a stable transient, whereas the kinetics in the near-infrared range show only evidence for the fast (i.e., $2.3 \times 10^{11}\ s^{-1}$) and the slow (i.e., $1.1 \times 10^{9}\ s^{-1}$) processes without giving rise to the stable transient. A plausible rationale implies the delocalization of the exTTF-centered excited state in aged **1c**.

Finally, a back transformation of aged solution **1c** in MCH into **1c** in MeOH, which is induced by dissolving aged **1c** in pure methanol, leads in line with the steady-state absorption measurements to exactly the same transient spectra that were recorded upon photoexcitation of **1c** in MCH, namely a fast decaying exTTF-centered transient. Importantly, when employing mixtures of MCH and MeOH evidence for both species emerged.

Information about the structural morphology of the solid obtained for aged **1c** stemmed from XRD, TEM, and SEM (scanning electron microscopy). In agreement with our initial hypothesis, self-assembled and homogeneous 3D mesoscopic helical fibers were seen in SEM images (Figure 3A and 3B). These fibers are composed of several tightly entwined—with

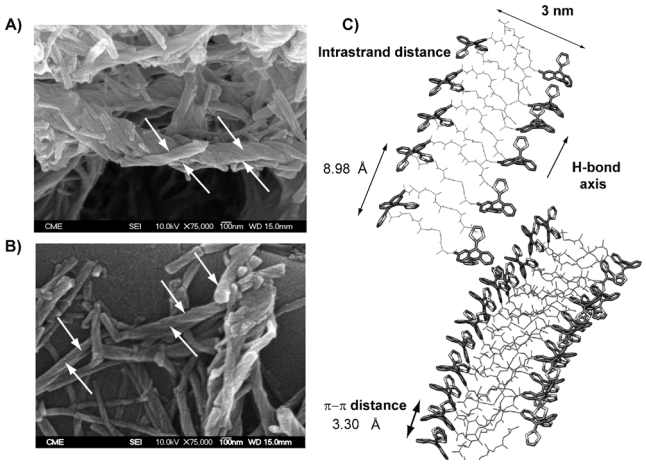

Figure 3. A and B) SEM-FEG images of aged **1c** that was precipitated from solution. C) Proposed tertiary structure (i.e., stacks of β-sheet arrangements) of **1c** in MCH.

one helical bias—fibrils possibly as a consequence of solvophobic collapse promoted in the solvents used for aging (Figure S13 in the Supporting Information).

These results suggest favorable interactions between adjacent supramolecular fibrils—previously formed by H bonds—possibly driven by efficiently π–π interacting exTTFs. It is important to remark that this is the first time that a concave aromatic system contributes effectively to the hierarchical growth of 3D helical fibers at mesoscopic length scales. A closer inspection displays rather large domains of twisted nanofibers oriented perpendicularly to the surface (Figure S14 in the Supporting Information).

In contrast to other reports on aromatic peptide systems, only a few nanotubes were observed.[13] Further investigations of these nanotubes by, for example, TEM document that they are formed by several stripes separated by a periodic distance of about 3 nm (Figure S14 in the Supporting Information). This is in accordance with the model for antiparallel β-sheet arrangements of **1c** (Figure S15 B in the Supporting Information).

XRD studies of the precipitate showed an intense and sharp reflection at 2.9 Å accompanied by a number of sharp and less-intense reflections at *d* spacings of 9.5, 8.98, and 3.30 Å (Figure S15 A in the Supporting Information). The two former *d* spacings are similar to those observed for surpramolecular β-sheet arrangements in other chromophore–peptide systems.[7] Here, the lack of the typical shorter interstrand reflections at *d* spacings in the range of 4–5 Å (i.e., 2θ values between 18 and 22°) is in accordance with our model of antiparallel β-sheet arrangements—relative to the H-bond axis (Figure 3 C) in concordance with the experimental FTIR results.

In this type of supramolecular arrangements, the repetitive distance is usually at around 0.9 nm.[14] It is remarkable that the XRD pattern shows clearly the distance of 3.30 Å, which we assign to π–π distances between exTTFs in the nanostructure. In fact, this value is in good agreement with previous calculations for π–π interacting exTTFs in supramolecular systems.[8] Notably, this is the first time that π–π distances between interacting exTTFs have been experimentally determined for 3D supramolecular nanoarchitectures.

In contrast to the above findings, aging of solutions of **1a** and/or **1b** under the same experimental conditions and concentrations used for **1c** resulted in the formation of white crystalline solids. Inspection by SEM showed the presence of long and straight planar belts for **1a** (Figure S16 A in the Supporting Information) and planar leaves for **1b** (Figure S16 B in the Supporting Information). In agreement with AFM results the observed nanoarchitectures did not show any helical signature.

In summary, we have shown the importance of the concave shape of exTTFs in the context of creating helical mesostructures. In particular, **1c** self-assembles by means of H bonding into a network of long chiral fibrils with helical features at the nanoscale. Importantly, exTTFs are, however, not interacting with each other in these secondary nanostructures.[15] The subsequent assembly of this secondary structure into a tertiary structure is based on the solvophobic collapse. The latter supports the entwinement into one helical bias of several fibrils to yield single handedness 3D superhelix/3D fibers at mesoscale. The experimentally found degree of order stems from stabilizing π–π interactions between the non-planar exTTFs. In **1c**, the lack of long alkyl side chains, together with the unusual hierarchical 3D growth, renders exTTFs—with their concave central cores—a powerful building block for growing well-defined helical nanostructures at the mesoscopic scale.

Moreover, aged **1c** shows in MCH distinct excited-state characteristics in terms of transient features and transient decays that contrast markedly from those seen for **1c** in MeOH. Among the latter stands out the excited-state delocalization, which goes hand in hand with a stabilization that exceeds the experimental time window of 8 ns.

The different nanostructures and morphologies—formed from the primary to the tertiary architectures—have been confirmed by a variety of complementary techniques (XRD, AFM, TEM, and SEM). The control over self-organizing sophisticated nanostructures endowed with electron-donating exTTFs paves the way, for example, to their integration in the preparation of photovoltaic devices,[16,17] where the control of the morphology at nano- and mesoscopic scales is a key aspect for higher energy conversion efficiencies.

Received: December 26, 2011
Revised: February 15, 2012
Published online: March 2, 2012

Keywords: electron transfer · helical structures · hydrogen bonds · π interactions · supramolecular chemistry

[1] a) J. H. van Esch, *Nature* **2010**, *466*, 193–194; b) S. Yagai, Y. Nakano, S. Seki, A. Asano, T. Okubo, T. Isoshima, T. Karatsu, K. Akihide, Y. Kikkawa, *Angew. Chem.* **2010**, *122*, 10186–10190; *Angew. Chem. Int. Ed.* **2010**, *49*, 9990–9994; c) M. A. Kostiainen, O. J. Kasyutich, J. L. M. Cornelissen, R. J. M. Nolte, *Nat. Chem.* **2010**, *2*, 394–399; d) L. Sánchez, R. Otero, J. M. Gallego, R. Miranda, N. Martín, *Chem. Rev.* **2009**, *109*, 2081–2091.

[2] a) M. V. D. Auweraer, F. C. D. Schryver, *Nat. Mater.* **2004**, *3*, 507 – 508.

[3] a) D. González-Rodríguez, A. P. H. J. Schenning, *Chem. Mater.* **2011**, *23*, 310 – 325; b) M. Gsänger, J. H. Oh, M. Könemann, H. W. Höffken, A-M. Krause, Z. Bao, F. Würthner, *Angew. Chem.* **2010**, *122*, 752 – 755; *Angew. Chem. Int. Ed.* **2010**, *49*, 740 – 743.

[4] a) D. Canevet, E. M. Pérez, N. Martín, *Angew. Chem.* **2011**, *123*, 9416 – 9427; *Angew. Chem. Int. Ed.* **2011**, *50*, 9248 – 9259; b) F. Giacalone, N. Martín, *Adv. Mater.* **2010**, *22*, 4220 – 4228; c) J. Wang, Y. Shen, S. Kessel, P. Fernandes, K. Yoshida, S. Yagai, D. G. Kurth, H. Möhwald, T. Nakanishi, *Angew. Chem.* **2009**, *121*, 2200 – 2204; *Angew. Chem. Int. Ed.* **2009**, *48*, 2166 – 2170.

[5] a) S. Xiao, M. Myers, Q. Miao, S. Sanaur, K. Pang, M. L. Steigerwald, C. Nuckolls, *Angew. Chem.* **2005**, *117*, 7556 – 7560; *Angew. Chem. Int. Ed.* **2005**, *44*, 7390 – 7394; b) Q. Chen, T. Chen, G. B. Pan, H. J. Yan, W. G. Song, L. J. Wan, Z. T. Li, Z. H. Wang, B. Shang, L. F. Yuan, J. L. Yang, *Proc. Natl. Acad. Sci. USA* **2008**, *105*, 16849 – 16854; c) D. Miyajima, K. Tashiro, F. Araoka, H. Takezoe, J. Kim, K. Kato, M. Takasata, T. Aida, *J. Am. Chem. Soc.* **2009**, *131*, 44 – 45.

[6] a) C. C. Lee, C. Grenier, E. W. Meijer, A. P. H. J. Schenning, *Chem. Soc. Rev.* **2009**, *38*, 671 – 683; b) J. D. Tovar, B. M. Rabatic, S. I. Stupp, *Small* **2007**, *3*, 2024 – 2028; c) T. Muraoka, H. Cui, S. I. Stupp, *J. Am. Chem. Soc.* **2008**, *130*, 2946 – 2947; d) L. S. Li, H. Jiang, B. W. Messmore, S. R. Bull, S. I. Stupp, *Angew. Chem.* **2007**, *119*, 5977 – 5980; *Angew. Chem. Int. Ed.* **2007**, *46*, 5873 – 5876.

[7] a) A. R. Hirst, S. Roy, M. Arora, A. K. Das, N. Hodson, P. Murray, S. Marshall, N. Javid, J. Sefcik, J. Boekhoven, J. H. van Esch, S. Santabarbara, N. T. Hunt, R. V. Ulijn, *Nat. Chem.* **2010**, *2*, 1089 – 1094; b) M. Manlung, J. Kuang, Y. Gao, Y. Zhang, P. Gao, B. Xu, *J. Am. Chem. Soc.* **2010**, *132*, 2719 – 2728; c) K. J. Channon, G. L. Devlin, S. W. Magennis, C. E. Finlayson, A. K. Tickler, C. Silva, C. E. MacPhee, *J. Am. Chem. Soc.* **2008**, *130*, 5487 – 5491.

[8] a) B. Adhikari, J. Nanda, A. Banerjee, *Chem. Eur. J.* **2011**, *17*, 11488 – 11496; b) E.-K. Schillinger, E. Mena-Osteritz, J. Hentschel, H. G. Boerner, P. Baeuerle, *Adv. Mater.* **2009**, *21*, 1562 – 1567; c) H. Shao, T. Nguyen, N. C. Romano, D. A. Modarelli, J. R. Parquette, *J. Am. Chem. Soc.* **2009**, *131*, 16374 – 16376; d) S. R. Diegelmann, J. M. Gorham, J. D. Tovar, *J. Am. Chem. Soc.* **2008**, *130*, 13840 – 13841.

[9] H. K. Murnen, A. M. Rosales, J. N. Jaworski, R. A. Segalman, R. N. Zuckermann, *J. Am. Chem. Soc.* **2010**, *132*, 16112 – 16119.

[10] J. L. López, C. Atienza, W. Seitz, D. M. Guldi, N. Martín, *Angew. Chem.* **2010**, *122*, 10072 – 10076; *Angew. Chem. Int. Ed.* **2010**, *49*, 9876 – 9880.

[11] J. C. M. van Hest, D. A. Tirrell, *Chem. Commun.* **2001**, 1897 – 1904.

[12] When a solution of **1c** in $CHCl_3$ or $C_2H_2Cl_4$ (where a network of fibrils is observed by AFM), is slowly left to dryness, and thus the dried film obtained is dispersed with MCH at 40 °C during about one hour, the UV/Vis spectra of the dispersion show exactly the same bathocromic shift observed when a solution of **1b** in a mixture of $CHCl_3$/MCH is aged over a week. The morphology observed for the precipitated, by SEM-FEG, is similar to that observed after aging a solution of **1c** in $CHCl_3$/MCH over a week (FEG = field emission gun).

[13] a) N. Amdursky, M. Molotskii, E. Gazit, G. Rosenman, *J. Am. Chem. Soc.* **2010**, *132*, 15632 – 15635; b) L. Adler-Abramovich, D. Aronov, P. Beker, M. Yevnin, S. Stempler, L. Buzhansky, G. Rosenman, E. Gazit, *Nat. Nanotechnol.* **2009**, *4*, 849 – 854.

[14] For X-ray studies in similar peptides sequences, see; a) E. D. T. Atkins in *Supramolecular and Colloidal Structures in Biomaterials and Biosubstrates*, Wordscientific, UK, **1999**.

[15] The repetitive distance through the H-bond axis (8.98 Å) in the secondary structure supports the mismatch between H-bond and π–π distances, thus avoiding the lateral zipper assembly in this secondary structure. This fact allowed controlling the sequential growth of the mesohelical architectures formed. For the zipper-type assembly see; a) R. Bhosale, A. Perez-Velasco, V. Ravikumar, R. S. K. Kishore, O. Kel, A. Gomez-Casado, P. Jonkheijm, J. Huskens, P. Maroni, M. Borkovec, T. Sawada, E. Vauthey, N. Sakai, S. Matile, *Angew. Chem.* **2009**, *121*, 6583 – 6586; *Angew. Chem. Int. Ed.* **2009**, *48*, 6461 – 6464; b) S. Bhosale, A. L. Sisson, P. Talukdar, A. Fürstenberg, N. Banerji, E. Vauthey, G. Bollot, J. Mareda, C. Röger, F. Würthner, N. Sakai, S. Matile, *Science* **2006**, *313*, 84 – 86.

[16] N. Martín, L. Sánchez, M. A. Herranz, B. Illescas, D. M. Guldi, *Acc. Chem. Res.* **2007**, *40*, 1015 – 1024.

[17] a) A. Sánchez-Díaz, M. Izquierdo, S. Filippone, N. Martín, E. Palomares, *Adv. Funct. Mater.* **2010**, *20*, 2695 – 2700; b) J. L. Delgado, P. A. Bouit, S. Filippone, M. A. Herranz, N. Martín, *Chem. Commun.* **2010**, *46*, 4853 – 4865; c) G. P. García-Belmonte, P. Boix, J. Bisquert, M. lenes, H. J. Bolink, A. La Rosa, S. Filippone, N. Martín, *J. Phys. Chem. Lett.* **2010**, *1*, 2566 – 2571; d) H. J. Bolink, E. Coronado, A. Forment-Aliaga, M. Lenes, A. La Rosa, S. Filippone, N. Martín, *J. Mater. Chem.* **2011**, *21*, 1382 – 1386.

